Observation of Stark shift in laser plasmas with a stigmatic, high-acceptance, high-resolution x-ray spectrograph

I. L. Beĭgman, Yu. Yu. Pokrovskiĭ, and E. N. Ragozin

P. N. Lebedev Physics Institute, Russian Academy of Sciences, 117924 Moscow, Russia
(Submitted 10 April 1996)
Zh. Éksp. Teor. Fiz. **110**, 1783–1796 (November 1996)

A stigmatic spectrograph for the wavelength region 170–190 Å is realized experimentally, including two identical normal-incidence multilayer mirrors ($\lambda_0 \simeq 180$ Å, $r = 2000$ mm) and a plane grazing-incidence diffraction grating. It is used to obtain spectra of multiply charged ions in laser produced plasmas. A resolving power of $\lambda/\delta\lambda = 24000$ is demonstrated with an astigmatic slit height of 16 μm and a reciprocal linear dispersion of 0.35 Å/mm. The profiles of the $2p-3s$ transition of the Mg IV ion at different distances from the target surface are analyzed. A comparison of the experimental intensity profiles with calculated ones indicates that the "red" wing of the lines fits a Holtsmark distribution with a quadratic Stark effect. It is shown that the theoretically calculated lineshape of the $2p^5\,^2P^0 - 2p^4(^3P)3s^2P$ transition of Mg IV is sensitive to the electron density n_e, which can be measured by this method at various distances from the target. © *1996 American Institute of Physics.* [S1063-7761(96)01611-3]

1. INTRODUCTION

Up to now the main instrument for spectroscopy in the soft x-ray range (30–300 Å) has been the concave diffraction grating.[1]

Research on x-ray lasers has stimulated the development of a new scheme in which a plane grating with a variable period is used together with a grazing-incidence focusing mirror.[2] This spectrometer is tuned by rotating the grating while the radiation detector is fixed (an interval of several Å is measured at each stop). The instrument maintains a resolution of $\simeq 30\,000$ over 130–210 Å. It has been used to observe a fivefold narrowing (to 10 mÅ) of the 206.38 Å line at the $(2p^5_{3/2}3p_{3/2})_2 - (2p^5_{3/2}3s_{1/2})_1$ lasing transition of neon-like Se XXV (Ref. 3), the absence of broadening of the same line owing to saturation,[3] and hyperfine splitting (28 mÅ) of the $J=0\rightarrow 1$, $3p\rightarrow 3s$ transition (145.9 Å) of neon-like Nb XXXII (Ref. 4).

A monochromator with a plane grating in a converging beam of synchrotron radiation reflected from an ellipsoidal mirror has been used to obtain a resolution of 11 000 at 190 Å (Ref. 5). This system was proposed by Petersen.[6]

Grazing-incidence schemes have extremely narrow acceptance angles ($\leqslant 10^{-4}$ sr) which cannot be increased without loss of resolving power.

Increasing the input solid angle and eliminating astigmatism require the use of normal-incidence optics, which has become possible in this wavelength range with the development of multilayer interference coatings. A multilayer Mo-Si coating ($\lambda_0 \simeq 156$ Å) deposited on a replica of a spherical ruled grating has made it possible to attain a resolution of 14 000 in a Rowland configuration after deduction of the slit apparatus function[7] (without this procedure the resolution was 9200).

We have developed a concept for high-resolution soft x-ray spectral devices that are stigmatic and have high acceptance, a combination of properties that were previously only characteristic of apparatus for the visible and ultraviolet regions. This makes it possible to record spectra with simultaneous high spatial and spectral resolution, and to determine the parameters of nonuniform plasmas in different spatial regions.

We have avoided the classical Rowland configuration with a concave diffraction grating and grazing incidence of the radiation. Our approach[8,9] is based on separating the functions of dispersion and focusing, as is traditional for visible spectroscopy, and on the ability of multilayer mirrors to form an image with a resolution close to the diffraction limit. Experimental confirmation of this will be given in Section 2.2. Normal-incidence multilayer mirrors are the focusing elements and the dispersive element is a plane grazing-incidence diffraction grating. This configuration combines high spectral resolution and the ability to obtain a stigmatic image of the entrance slit. A point on the entrance slit, which is vertical, is imaged onto the spectral (horizontal) focal curve in the form of a vertical segment with a height on the order of hundredths of a millimeter. In a first realization of this scheme (two multilayer spherical Mo–Si mirrors with $D = 40$ mm, $\lambda_0 \simeq 135$ Å, and $r = 1000$ mm, and a plane 1200 groove/mm 30 mm (height)$\times$28 mm (width) diffraction grating), a spectral resolution of $4 \cdot 10^3$ was obtained with a vertical astigmatism of 35 mm.[10]

In this paper we describe a new device of this type for wavelengths of 170–190 Å. It has been used to record spectra of Mg, Fe, F, and V ions excited during irradiation of solid targets with radiation from a periodically pulsed laser at irradiances of up to $q_L \sim 10^{12}$ W/cm^2. A spectral resolution of $\lambda/\delta\lambda = 24\,000$ was obtained. The high resolution and the stigmatic imaging make it possible to observe the quadratic Stark effect in the $2p^43s$ levels of the Mg IV ion owing to the electrical microfields in the dense plasma.

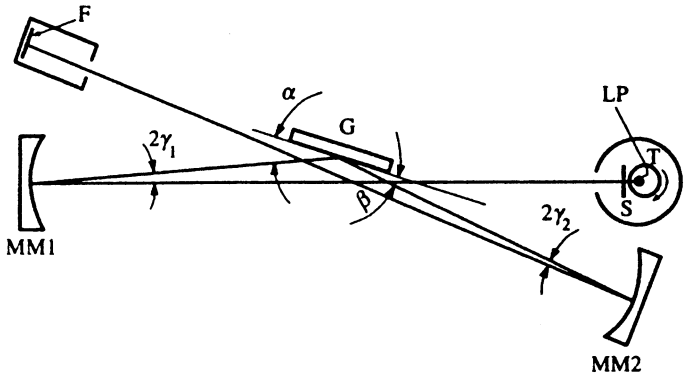

FIG. 1. Optical layout of the spectrograph.

2. DESIGN AND OPTICAL ELEMENTS

2.1. Optical configuration of the spectrograph

The optical configuration of the stigmatic spectrograph is shown in Fig. 1. The normal-incidence multilayer mirrors MM1 and MM2 ($\lambda_0 \simeq 180$ Å, $r=2000$ mm, $D=60$ mm) served, respectively, as the objectives for the entrance collimator and camera. The dispersing element was a plane diffraction grating G with a gold coating ($p=1800$ groove/mm, blaze angle $\Omega=7°$, height of grooves $H=30$ mm, width of grooved portion $W=40$ mm) mounted for grazing incidence. The second ($m=-2$) outer order of the spectrum was used. The radiation was detected by an UF-4 plate (F) with a resolution of 170 lines/mm.

A laser produced plasma (LP) was produced by the second harmonic ($\lambda=0.54$ μm) of the output pulse from a single-mode Nd:$YAlO_3$ laser with a passive Q-switch (the laser pulse energy at the target was up to 0.15 J; its duration was 5 ns).[11] The beam was focussed by a fused quartz lens ($f=106$ mm) onto the surface of a rotating target (T) several millimeters from the entrance slit (S). Targets made of materials with different nuclear charges were used. The size of the focal spot was varied. In order to prevent parasitic illumination, the target and entrance slit assemblies were mounted in a light-tight case with openings for the laser light and soft x-ray radiation. All of the optical elements of the spectrograph, target, focussing lens, and steering mirror were fastened to a vibrationally isolated duraluminum optical slab (size 1100×580 mm^2). The spectrograph was placed in a large vacuum chamber with a diameter of 0.9 m and a length of 4 m equipped with oil-free pumps.[12] The laser light passed through a window with an antireflection coating at $\lambda=0.53$ μm mounted in the end flange of the vacuum chamber.

The dispersing element serves as the aperture stop of the spectrograph; thus, the theoretical resolving power is

$$\mathscr{R}_0 = mN = mpW = 1.44\cdot 10^5.$$

The principal aberration of this optical system which affects the resolution is meridional coma. When off-axis angles $\gamma_1=0.77°$ and $\gamma_2=1.07°$ are used, the combined aberration in the dispersion direction at the center of the working region of the spectrum (180 Å) is 4 μm. The aberration in the direction of the slit height is mainly determined by the astigmatism and for the chosen grating groove height it is 16 μm.

The low reciprocal linear dispersion $d\lambda/dl$ was a result of using the grating in the outer orders. For $\alpha=22°$ and $\beta=7.26°$ (the grazing α and diffraction β angles are taken relative to the grating surface) it is 0.35 Å/mm. Table I shows the spectral intervals $\delta\lambda$ that are permitted by the dispersing element, optical geometry, and detector. The combined dispersion spot is then 8 μm and the maximum resolution (with an infinitely narrow entrance slit) is $\mathscr{R}=64000$.

The system was aligned with a He–Ne laser ($\lambda\approx0.63$ μm) with the aid of an optical-mechanical goniometer when the diffraction grating was replaced by a glass plate of equivalent thickness and larger width ($W=100$ mm). The alignment of this kind of system with visible light is discussed in more detail elsewhere.[10]

2.2. Normal-incidence multilayer mirrors

The multilayer Mo–Si coatings were deposited by single pass magnetron sputtering in an argon atmosphere at the Kharkov Polytechnical Institute.[13]

In order to study the spectral characteristics of multilayer mirrors a method for topographic study of the mirrors has been developed[13–15] which can be used to observe the reduction in the resonant wavelength λ_0 toward the edge of the aperture, which is asymmetric relative to the center of the aperture of the multilayer mirror and the reduction $\Delta\lambda_{1/2}$ in the half width of the local reflection curve, as well as to demonstrate the effect of the resonance reflection curve $R(\lambda,\mathbf{r})$ ($\mathbf{r}$ is the coordinate in the aperture) of the multilayer mirror on the integrated reflection coefficient of the pair of mirrors.[16] Because of the resonant character of the reflection from a multilayer mirror, the working bandwidth of the ap-

TABLE I. Limiting spectral resolutions owing to diffraction $(\delta\lambda)_{dif}$, meridional coma aberration $(\delta\lambda)_{coma}$, the spatial resolution of the UF-4 x-ray film $(\delta\lambda)_{film}$, and the combined effect of these factors $\sqrt{\Sigma(\delta\lambda)^2}$.

$(\delta\lambda)_{dif}$, mÅ	$(\delta\lambda)_{coma}$, mÅ	$(\delta\lambda)_{film}$, mÅ	$\sqrt{\Sigma(\delta\lambda)^2}$, mÅ
1.25	1.4	2.1	2.8

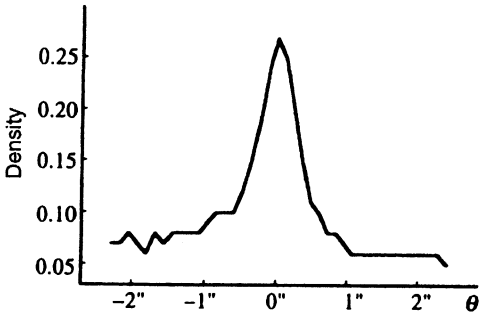

FIG. 2. An image of a slit with subsecond angular resolution produced by a normal-incidence multilayer x-ray mirror. (θ is the angular size of the image of the slit.)

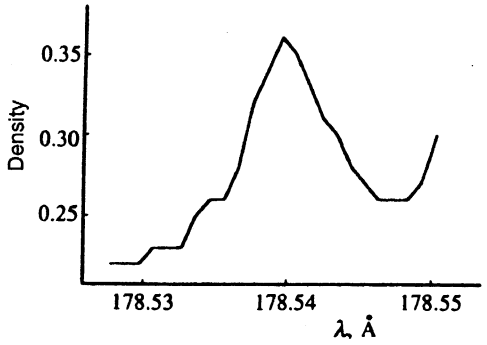

FIG. 3. The $\lambda = 178.540$ Å F IV line with a width of 7.4 mÅ recorded during irradiation of a $(CF_4)_n$ target.

paratus is limited to $\lambda_0 \pm \Delta\lambda_{1/2}$, where $\lambda_0 = 2dn$ is the wavelength at which the reflection coefficient of the multilayer mirror is highest for normal incidence and $\Delta_{1/2}$ is the full width at half maximum (FWHM) of the spectral reflection coefficient.

The focal properties of the multilayer mirrors have been studied elsewhere.[17] Quasi-monochromatic images of a two-dimensional test object and slit, created with the aid of the focusing multilayer mirror, were recorded with subsecond angular resolution on a type UF-n x-ray photographic plate developed at NIIKhIMFOTOPROEKT, Inc. This film provides a resolution of at least 350 lines/mm. Figure 2 shows a microdensitometer trace of the image of a five-micron slit obtained with a 1:1 magnification with the aid of an Mo–Si mirror ($D = 25$ mm). An analysis of this image (including the grain size of the photographic emulsion, 1–1.5 μm) showed that the image of a point source created by the mirror had a size of less than 2.5 μm or 0.3″ (at least in terms of width). The closeness of the intrinsic resolution of the multilayer mirror to the diffraction limit ($\lambda/D \approx 0.15''$) serves as an experimental justification for the use of multilayer normal-incidence x-ray mirrors in high and ultra-high resolution spectroscopy.

2.3. Resolving power of the instrument

The experimental results were processed using an automatic scanning microdensitometer with a laser displacement measurement device.[18] The spectrophotometer traces presented in this paper were scanned with a step size of $8\lambda/2$, where $\lambda \sim 0.63$ μm is the wavelength of the He–Ne laser, while the microdensitometer trace of Fig. 2 was obtained with a scan step size of $4\lambda/2$.

Figure 3 shows an unsmoothed fragment of a spectrum obtained by irradiating a teflon $(CF_4)_n$ target and taken at a height of 145 μm. This is the $2p4s - 2p^2$ 178.540 Å line of the F IV ion which lies between two strong lines of the F V ion.[19] The overall linewidth at half maximum is 7.4 mÅ, which gives the instrument a resolving power of $\lambda/\delta\lambda = 24000$.

3. STARK BROADENING IN LASER PRODUCED PLASMAS

3.1. Experimental profiles of an Mg IV line

Figure 4 shows a photograph of part of the spectrum of Mg IV (four components of the multiplet splitting of the resonant $2p^5 - 2p^4(^3P)3s$ transition between the $^2P^0 - ^2P$ terms), obtained in 900 laser shots, which shows clearly the high stigmatic quality of the apparatus. A level diagram is shown in Fig. 5.

The "blue" dip, which is present in the lines at the target surface (see Fig. 4) is explained by reabsorption of the radiation in the plasma. Descriptions of this effect in an optically thick plasma[20] and in an expanding laser-produced plasma[21] have been given elsewhere. Thus, with high expansion velocities the dip is assumed to exist even in an optical thin plasma.[21] We believe that the most probable reason for the blue dip is absorption in the outer, colder layer of the expansion cone of the plasma which has a velocity component in the direction of the observer. The unshifted positions of the lines essentially coincide with the center of the reabsorption lineshape at the target surface. With increasing distance from the target, the central frequency of the reabsorption is shifted to shorter wavelengths owing to the Doppler effect and reproduces the well-known saturation of the expansion velocity which has been observed spectroscopically before.[22] Because of the uncertainty in the reemission function, in the expansion velocities of the plasma, and in the sizes of the absorbing region, this effect was not examined quantitatively.

Densitometer traces of the Mg spectrum obtained on an automatic scanning microdensitometer[18] are shown in Figs. 6 and 7. Density was converted to exposure using the blackening curve for the UF-4 plate. Then the background, which was the same for all the densitometer traces, was removed additively and the spectrum was Fourier-filtered to eliminate the film noise. It is convenient to compare the calculated lineshapes with the Fourier-filtered experimental profiles (smooth curves in Figs. 6 and 7).

3.2. Pressure-broadening mechanisms

The interaction with the nearest $3p$ levels owing to the electric microfield of the electrons and ions in a laser-produced plasma causes a shift and an effective broadening

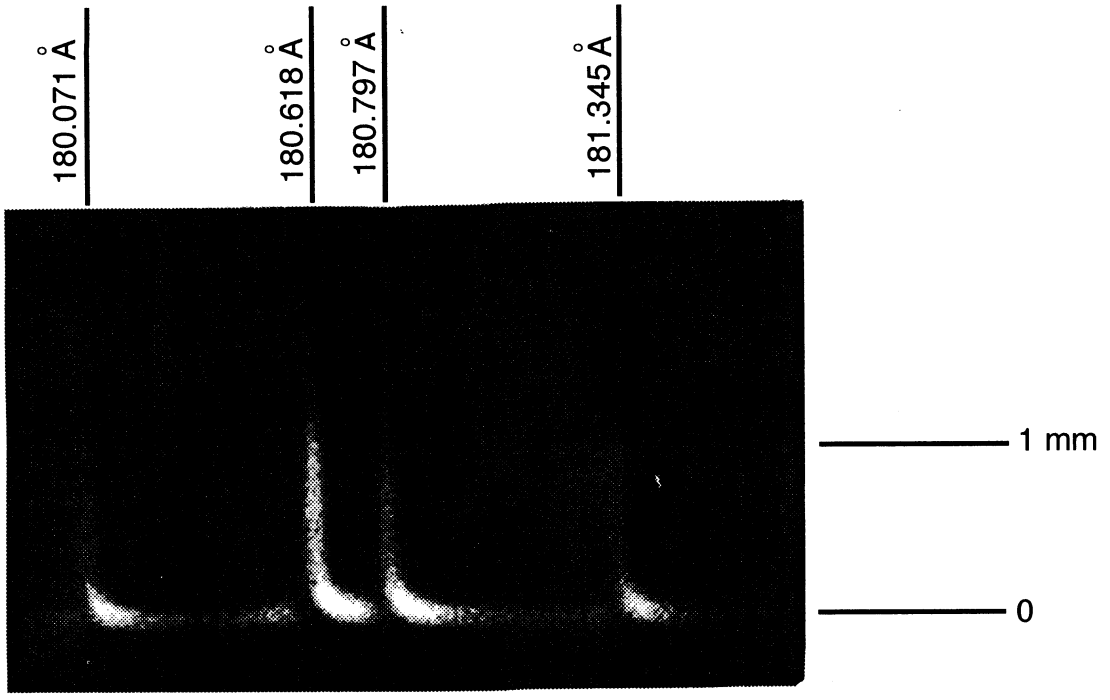

FIG. 4. Photograph of a segment of the spectrum of Mg IV ($2p^5-2p^4 3s$ transition). The shift in the resonance lines is caused by the quadratic Stark effect. The dips are caused by absorption in the cold outer region of the laser produced plasma; their shift to shorter wavelengths is explained by the Doppler effect in the expanding plasma.

of the upper $3s$ levels. The relationship between the time a perturbing particle interacts with this system and the reciprocal of the frequency shift necessitates use of either a collisional or quasistatic mechanism for describing the lineshape. In the case of broadening by the electrons, the integrated intensity of the line is almost completely concentrated in the collisional region and is fit by a Lorentz profile. Ion broadening is mainly quasistatic and produces a long-wavelength ("red") wing in the profile. Both mechanisms are statistically independent, so that, in general, the lineshape is described by a convolution of Lorentz and quasistatic distributions.

The lower level of the transition being considered here is the ground state, so its broadening and shift can be neglected.

3.3. Ion broadening

The electric field $\mathscr{E}$ created by the ensemble of randomly distributed charged particles in the ideal-gas approximation (neglecting the mutual correlation in the positions of the ions) is described by the Holtsmark function $H(\beta)$,[23]

$$W_H(\mathscr{E})d\mathscr{E}=H(\beta)d\beta, \quad \beta=\mathscr{E}/\mathscr{E}_0,$$
$$\mathscr{E}_0=2.6(Z-1)eN_Z^{2/3},$$
$$H(\beta)=\frac{2}{\pi\beta}\int_0^\infty x\sin x\exp\left[-\left(\frac{x}{\beta}\right)^{2/3}\right]dx, \tag{1}$$

where N_Z is the density of the perturbing ions and the charge of the atomic core (spectroscopic symbol) is $Z=4$. (We assume that the maximum in the density distribution of the ions corresponds to Mg IV.)

The function $H(\beta)$ can be approximated by the expression

$$H(\beta)=a\frac{\beta^2}{1+c\beta^{3.5}}\frac{1+bd\beta}{1+(d\beta)^2}, \tag{2}$$

which is asymptotically exact both for $\beta\ll 1$,

$$H(\beta)\approx a\beta^2, \quad a=4/3\pi,$$

and for $\beta\gg 1$,

$$H(\beta)\approx\frac{ab}{cd}\beta^{-5/2}, \quad b=1.496\frac{cd}{a},$$

$$c=0.06, \quad d=0.85.$$

A comparison with exact numerical data[24] shows that the error is less than 3–5% in the region $\beta\approx 1$.

The shift ΔE in the level of a non-hydrogen-like ion acted on by an external electric field $\mathscr{E}$ is determined by the quadratic Stark effect,

$$\Delta E=\sum_{\gamma'}\frac{|\langle\gamma|\mathscr{E}\mathbf{D}|\gamma'\rangle|^2}{E_\gamma-E_{\gamma'}}, \tag{3}$$

where $\mathbf{D}=e\mathbf{r}$ is the dipole moment operator, γ, E_γ, and γ', $E_{\gamma'}$ are the quantum numbers and energies of the perturbed and perturbing levels, respectively.

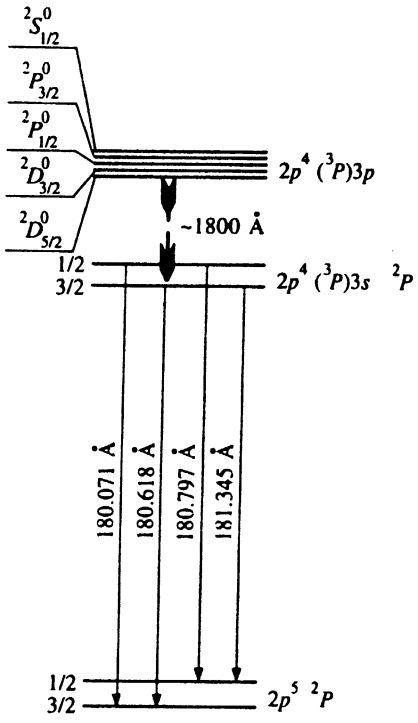

FIG. 5. A diagram of the resonance transitions of Mg IV.

Then, using the approximation of a hydrogen-like ion for calculating the matrix element and average distance ΔE_{av} to the perturbing level, we obtain the shift in the upper s-level:

$$\Delta E = 3\,\mathrm{Ry}\,\frac{\mathrm{Ry}}{\Delta E}\left(\frac{a_0^2}{e}\mathscr{E}\right)^2\frac{n_*^2(n_*^2-1)}{Z^2}, \tag{4}$$

where $n_*=2.3$ is the effective principal quantum number, $a_0=\hbar^2/me^2=0.5292\cdot 10^{-8}$ cm is the atomic unit of length, e is the electronic charge, Ry is the Rydberg constant, and

$$\frac{1}{\Delta E_{av}}\equiv\frac{1}{N}\sum_{i=1}^{N}\frac{1}{\Delta E_i},$$

where the sum was taken over the five perturbing levels of the nearest $3p$ level.

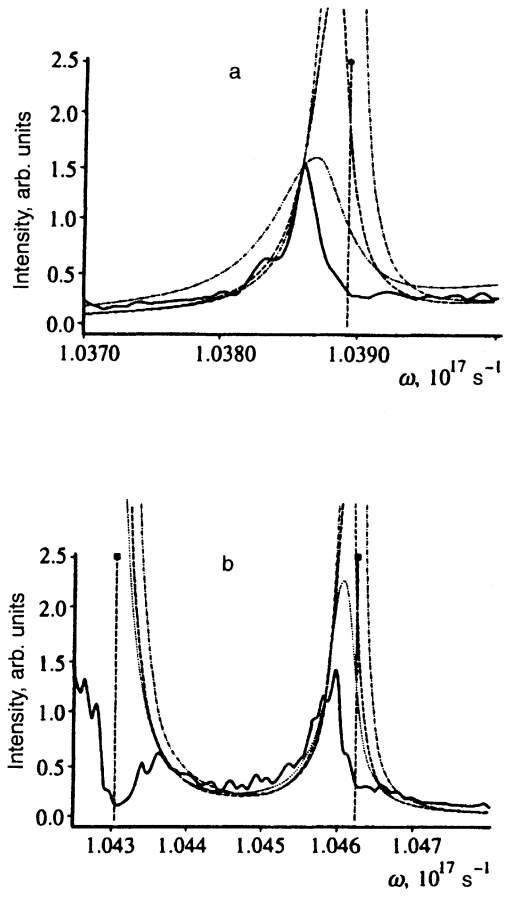

FIG. 7. Fragments of the microdensitometer traces of Fig. 6a. The vertical lines denote the position of the center of the unshifted line which was found by scanning at a distance of 700 μm from the target surface (Fig. 6b). The broken curves are theoretical profiles obtained for $n_e=2.5\cdot 10^{20}$ cm^{-3} (dot-dashed with two points), $n_e=1.8\cdot 10^{20}$ cm^{-3} (dotted), $n_e=1.3\cdot 10^{20}$ cm^{-3} (dashed), and $n_e=0.5\cdot 10^{20}$ cm^{-3} (dot-dashed).

The intensity distribution in the line is proportional to the statistical weight of the configuration of the perturbing particles for which the frequency of the atomic oscillator lies within the interval $\omega,\omega+d\omega$:

$$I(\omega)d\omega=I_0W(\mathscr{E})d\mathscr{E}. \tag{5}$$

Finally,[23] for quasistatic broadening by the ions we obtain ($\omega<\omega_0$)

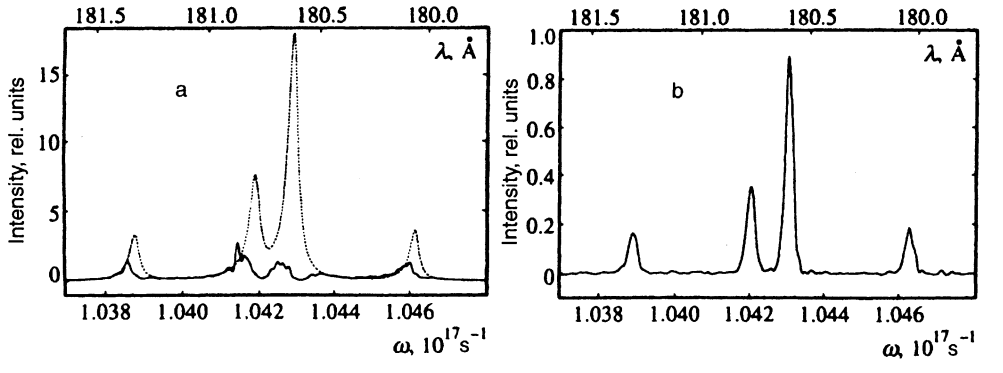

FIG. 6. Spectrum of the $2p^4(^3P)3s^2P-2p^5\ ^2P^0$ transition of Mg IV. The microdensitometer traces were obtained by scanning the spectrum of Fig. 4 at different distances h from the target surface: (a) $h=0$, (b) $h=700$ μm. The smooth curves are Fourier filtered experimental spectra with the background subtracted; the dashed curve is a profile calculated using Eq. (7) for $n_e=1.3\cdot 10^{20}$ cm^{-3}.

TABLE II. Excitation rates for the $3s-3p$ transition.

kT_e/Ry	16	8	4	2
T_e, eV	217.60	108.80	54.40	27.20
$Z^3\langle v\sigma\rangle_{3s-3p}$, 10^{-5} cm^3/s	0.83	0.98	1.2	1.4

$$I(\omega)=\frac{I_0 a}{2\Delta\omega_H}\frac{\left(\frac{\omega_0-\omega}{\Delta\omega_H}\right)^{1/2}+bd\left(\frac{\omega_0-\omega}{\Delta\omega_H}\right)}{\left(1+d^2\frac{\omega_0-\omega}{\Delta\omega_H}\right)\left[1+c\left(\frac{\omega_0-\omega}{\Delta\omega_H}\right)^{1.75}\right]}, \quad (6)$$

where

$$\Delta\omega_H=\frac{3}{4}(2.6)^2\frac{\hbar^3}{m^2}\frac{1}{\Delta E_{av}}n_*^2(n_*^2-1)\frac{(Z-1)^2}{Z^2}N_Z^{4/3},$$

and ω_0 is the frequency of the unshifted line.

3.4. Electron collisional broadening

Line broadening by collisions with electrons is described by the well known Lorentz distribution. The linewidth $\gamma=n_e\langle v\sigma\rangle$ is determined primarily by the rate of the transition to the nearest $3p$ level. Table II shows the calculated excitation rates $Z^3\langle v\sigma\rangle_{3s-3p}$ for the ions at different electron temperatures T_e using the program ATOM.[25] Since the electron temperature has been estimated to be $T_e\approx 50$ eV for similar experimental conditions,[14] in the calculations we have taken $Z^3\langle v\sigma\rangle_{3s-3p}=1.2\cdot 10^{-5}$ cm^3/s.

Numerical calculations indicate that inelastic collisions play a fundamental role.

3.5 Combined broadening

The convolution over the interval $(0,\omega_0)$ of a standard Lorentz profile with the profile (6) corresponding to quasistatic ion broadening describes the combined effect of the electrons and ions and can be written in the form

$$I(\omega)=\frac{\gamma I_0}{\pi(\Delta\omega_H)^2}\frac{ab}{cd}\times\int_0^{(\omega_0/\Delta\omega_H)^{1/4}}\frac{t^5(t^2+1/bd)dt}{(t^4+1/d^2)(t^7+1/c)[(t^4-k)^2+l^2]}, \quad (7)$$

where

$$k=\frac{\omega_0+\Delta-\omega}{\Delta\omega_H}, \quad l=\frac{\gamma}{2\Delta\omega_H},$$

and Δ is the line shift owing to collisions with electrons, while γ and $\Delta\omega_H$ have been defined above.

The long-wavelength wing of the line profile (7) has a Holtsmark asymptote $(\omega_0-\omega)^{-7/4}$ and the short-wavelength wing has a Lorentz asymptote $(\omega-\omega_0)^{-2}$. Thus, we have an asymmetric lineshape that is shifted toward lower frequencies relative to the unperturbed frequency ω_0.

We should point out why the Doppler broadening associated with the random motion of the particles has been neglected in Eq. (7). The ion temperature in a laser-produced plasma is, as a rule, substantially lower than the electron temperature owing to the long electron–ion relaxation time. As an estimate, let us take $T_i\sim 0.1T_e$. Then the relative Doppler width is $\Delta\omega_p/\omega\sim 10^{-5}$, or an order of magnitude less than the linewidth at the target surface.

TABLE III. The parameter $g_i f_{ij}$ for the multiplet components of the Mg IV $2p^5\ ^2P^0-2p^4(^3P)3s^2P$ transition calculated with the ATOM program[25] and GRASP-2 program[26] (with Coulomb and Babushkin gauges).

J_{low}	J_{up}	ATOM (LS-coupling)	GRASP-2 (B)	GRASP-2 (C)
3/2	1/2	0.057	0.046	0.064
1/2	1/2	0.11	0.089	0.12
3/2	3/2	0.29	0.23	0.32
1/2	3/2	0.059	0.041	0.058

3.6. Comparison with experiment

The theoretical lineshapes shown as dotted curves in Figs. 6 and 7 are superpositions of the four components of the multiplet, each of which was calculated using Eq. (7) and has been multiplied by $g_i f_{ij}$ in the sum, where g_i is the statistical weight of the initial (upper) level and f_{ij} is the oscillator strength of the given component of the multiplet. Acccording to estimates, the probability of the radiative transitions is two orders of magnitude smaller than the nonradiative transition probability. Table III shows values of the parameter $g_i f_{ij}$ calculated using the ATOM program[25] in the LS-coupling approximation and the GRASP-2 program[26] using a Dirac-Fock method with Coulomb and Babushkin gauges. In the calculated spectra of Figs. 6 and 7 we have used the relative values of $g_i f_{ij}$ given by the GRASP-2 program with a Babushkin gauge. These values are roughly the same in all three cases.

The fact that the intensities of the multiplet components at a distance of 700 μm from the target surface are related to one another as $g_i f_{ij}$ (cf. Fig. 6b and the dashed curve of Fig. 6a) indicates that the plasma in this region is optically thin and that the unshifted frequency ω_0 can be determined from its emission spectrum (in Figs. 7a and 7b these frequencies are denoted by vertical dashed lines). Thus, the absolute shift in the maximum is not a free parameter.

As can be seen from Table II, the Lorentz width γ depends very weakly on the electron temperature T_e, while the Holtsmark width $\Delta\omega_H$ does not depend explicitly on T_e (only through the ion density N_Z, i.e., through $n_e=3N_Z$).

The electron density n_e is the only parameter that determines the lineshape. By varying the amplitude of the theoretical spectrum and comparing it with the experimental profiles it is possible to determine the electron density in the laser-produced plasma at different distances from the target.

Table IV lists the electron densities and the errors in these determinations. The upper bound on n_e was determined from the unperturbed long-wavelength edge of the 181.345 Å line (see Fig. 7a) and the lower bound, from the short-wavelength edge of the 180.618 Å line (see Fig. 7b). Each of the theoretically calculated profiles (broken curves in Figs. 7 and 6a) was multiplied by an arbitrary factor and compared

TABLE IV. Density n_e of the laser produced plasma as a function of distance to the target.

h, μm	0	30	70
n_e, 10^{20} cm^{-3}	$1.3^{+0.5}_{-0.8}$	$1.0^{+0.3}_{-0.5}$	$0.8^{+0.5}_{-0.4}$

with the experimental Fourier-filtered profile. Thus, the criterion for determining n_e was not a quantitative parameter (linewidth, shift, or intensity ratio), but a qualitative parameter (the shape of the profile). In Fig. 7a, for example, it is quite clear that when n_e is doubled the line profile changes so much that it cannot be matched to the experimental profile for any value of the arbitrary multiplier.

4. CONCLUSION

A stigmatic high-resolution spectrograph employing normal-incidence multilayer mirrors and a plane reflection diffraction grating has been used to study the spectra of a laser-produced plasma in the soft x-ray range. A resolving power of $\lambda/\delta\lambda = 24\,000$ has been obtained at a wavelength of $\lambda = 178.5$ Å with a reciprocal linear dispersion of 0.35 Å/mm and an astigmatism of 16 μm. Line broadening and shifts owing to the quadratic Stark effect have been observed. A method has been developed for determining the electron density n_e at various distances from the target.

The unique combination, for the soft x-ray range, of high resolution and stigmatic imaging make this new type of spectrograph attractive, especially for x-ray plasma diagnostics. The high acceptance of the instrument means that it can be used for relatively low brightness sources, not just ultrabright sources of soft x-rays (e.g., the emission from x-ray lasers). It is also important that the low reciprocal linear dispersion ($d\lambda/dl \approx 0.35$ Å/mm) permits spectral and spatial resolution with this device when two-dimensional CCD arrays are used as detectors.

We thank M. A. Mazing for interest in this work and for useful discussions; L. A. Vainshtein and E. A. Yukov[1)] for discussing the experimental results and for assistance; V. I. Azarov, N. N. Kolachevskii, and M. M. Mitropol'skii for assistance in doing the experiments and processing the spectroscopic data; V. V. Kondratenko, A. I. Fedorenko, and S. A. Yulin for assistance; I. Grant for the opportunity to use the GRASP-2 program; and, A. I. Sharkov for depositing the coating on the diffraction grating.

This work was supported by the International Scientific-Technical Center (projects No. 021 and 076). The studies reported in this paper were made possible in part by the support of the Russian Fund for Fundamental Research (Project Code No. 94-02-5371), as well as by the combined support of the International Science Foundation and the Russian government (Grant No. MKA300).

[1)]Deceased

[1] A. N. Zaidel and E. Ya. Shreider, *Vacuum Spectroscopy and its Applications* [in Russian], Nauka, Moscow (1976).
[2] M. C. Hettrick, J. H. Underwood, P. J. Batson, and M. J. Eckart, Appl. Opt. **27**, 200 (1988).
[3] J. A. Koch, B. J. MacGowan, L. B. Da Silva *et al.*, Phys. Rev. Lett. **68**, 3291 (1992).
[4] J. Nilsen, J. A. Koch, J. H. Scofield *et al.*, Phys. Rev. Lett. **70**, 3713 (1993).
[5] M. Domke, A. Puschmann, C. Xue *et al.*, Synchr. Rad. News **3**(5), 21 (1990).
[6] H. Petersen, Opt. Commun. **40**(6), 402 (1982).
[7] M. P. Kowalski, J. F. Seely, W. R. Hunter *et al.*, Appl. Opt. **32**, 2422 (1993).
[8] E. N. Ragozin, in *IAU Colloq. 115: High Resolution X-ray Spectroscopy of Cosmic Plasmas*, 22–25 Aug. 1988, Cambridge Univ. Press (1990), p. 380.
[9] E. N. Ragozin, Trudy FIAN **196**, 123 (1989).
[10] E. N. Ragozin, N. N. Kolachevsky, M. M. Mitropolsky *et al.*, Phys. Scripta **47**, 495 (1993).
[11] I. A. Zhitnik, S. V. Kuzin, M. M. Mitropolskiĭ *et al.*, Kvant. Elektron. **20**, 89 (1993) [Quantum Electron. **23**, 76 (1993)].
[12] M. M. Mitropol'skiĭ, V. A. Slemzin, and N. K. Sukhodrev, Preprint No. 186, FIAN, Moscow (1989).
[13] N. N. Kolachevskiĭ, V. V. Kondratenko, M. M. Mitropol'skiĭ *et al.*, Kratkie soobshcheniya po fizike FIAN, No. 7–8, p. 51 (1992).
[14] E. N. Ragozin, N. N. Kolachevsky, M. M. Mitropolsky *et al.*, Proc. SPIE **2012**, 209 (1993).
[15] N. N. Kolachevskiĭ, V. V. Kondratenko, M. M. Mitropol'skiĭ *et al.*, Kratkie soobshcheniya po fizike FIAN, No. 11–12, p. 70 (1994).
[16] E. N. Ragozin, N. N. Kolachevsky, M. M. Mitropolsky *et al.*, Proc. SPIE **2520**, 309 (1995).
[17] N. N. Kolachevskiĭ, M. M. Mitropol'skiĭ, V. V. Kondratenko *et al.*, Kratkie soobshcheniya po fizike FIAN, No. 5–6, p. 56 (1994).
[18] V. I. Azarov, A system for automatic processing of the photospectrograms, Preprint, Institute of Spectroscopy, Troitsk (1991).
[19] E. N. Ragozin, N. N. Kolachevsky, M. M. Mitropolsky *et al.*, Proc. SPIE **2520**, 297 (1995).
[20] N. G. Preobrazhenskiĭ, *Spectroscopy of Dense Plasmas* [in Russian], Nauka, Novosibirsk (1971).
[21] F. E. Irons, J. Phys. B: Atom. Molec. Phys. **8**, 3044 (1975).
[22] G. V. Peregudov and E. N. Ragozin, Sov. Phys. JETP Lett. **28**, 26 (1978).
[23] I. I. Sobelman, *Atomic Spectra and Radiative Transition*, Springer, New York (1979).
[24] L. A. Vainshtein, I. I. Sobelman, and E. A. Yukov, *Excitation of Atoms and Broadening of Spectral Line*, Springer, New York (1981).
[25] L. A. Vainshtein and V. P. Shevelko, *Structure and Characteristics of Ions in Hot Plasmas* [in Russian], Nauka, Moscow (1986).
[26] K. A. Dyall, I.-P. Grant, C. T. Johnson *et al.*, Comp. Phys. Comm. **55**, 425 (1989).

Translated by D. H. McNeill